

---

# Plasma-Ion-Assisted Coatings for 15-fs Laser Systems

## Introduction

Interest in femtosecond (fs)-pulsed, high-intensity laser facilities continues to grow as evidenced by numerous large laser projects, including the Astra Gemini and Vulcan 10PW lasers at the Rutherford Appleton Laboratory, the Scarlet laser at Ohio State, the planned construction of the Apollon Laser Facility, the Extreme Light Infrastructure (ELI) project, and the planned construction of the Multi-Terawatt Optical Parametric Amplifier Line (MTW-OPAL) laser at the University of Rochester.<sup>1–5</sup> These laser facilities are designed to explore matter interactions with ultra-intense laser sources, necessitating the construction of high-energy, short-pulse lasers with ever-higher peak powers. Optical coatings capable of withstanding such high incident laser intensity must be developed and deposited on substrates at the beam size of these lasers, making it possible to create such laser facilities and achieve the desired laser intensities.

Electron-beam evaporation remains the primary optical coating technology for large-scale lasers, such as those used for inertial confinement fusion (ICF), although most coatings have been used for nanosecond (ns)- and picosecond (ps)-pulse durations.<sup>6–11</sup> The addition of plasma-ion-assisted deposition (PIAD) has also been successfully demonstrated for fabricating coatings for high-power lasers.<sup>12,13</sup> Since these technologies are readily available and have been proven successful in the production of meter-scale, high-laser-damage-threshold coatings, plasma-assisted evaporation has been selected for this development effort of large-aperture optical coatings for 15-fs applications.

Coatings for laser systems that must deliver compressed pulses of less-than-1-ps duration require more-stringent performance criteria than those for longer pulses, based on the wavelength-dependent group delay (GD), the group-delay dispersion (GDD), and higher-order dispersion terms resulting from the reflected phase from the coated surface. Spatial variations in the reflected phase over the optic aperture are particularly challenging since such variations cannot generally be compensated by other components in the laser system. Optical coatings for femtosecond applications require not only a controlled, smooth

GDD over the required bandwidth to maintain the temporal profile of the pulse but also a smooth phase across the optic aperture to provide consistent performance over the beam, so any coating technology pursued must be able to provide such performance over the desired substrate aperture.

This work describes the development of high-laser-damage-threshold coatings for a 15-fs optical parametric chirped-pulse-amplification (OPCPA) laser system having a spectral bandwidth of 810 to 1010 nm using plasma-ion-assisted electron-beam evaporation.<sup>5</sup> The high degree of sensitivity of controlled-phase coating designs requires that the coating performance be independent of relative humidity, thereby creating a need for a densified coating process producing low-porosity films. The use of optical coatings with high-peak-power laser systems necessitates high laser-damage thresholds, limiting potential coating materials and electric-field distributions within the coating structure. In addition, spatial control of phase on reflection for the entire bandwidth is critical to preserving pulse length; coating deposition must be quite uniform, without high-spatial-frequency changes in the reflected phase of the coating. Coating requirements are demonstrated on 10-in. substrates, although the deposition process was designed to be scalable for use on meter-class laser system components, such as those in use at the National Ignition Facility, the Laser MégaJoule Facility, the OMEGA EP Laser System, and other fusion-class lasers.<sup>6–11</sup>

## Background

The primary challenge when depositing coatings for femtosecond pulses is to preserve the compressibility of the temporal pulse. The consequence of a 15-fs temporal pulse is that its physical length is of the order of the thickness of an optical interference coating; in this case, the physical length of a 15-fs pulse would be 4.5  $\mu\text{m}$ , or approximately five wavelengths of light. Each wavelength in the spectral bandwidth has a relative GD when reflecting from a multilayer optical coating, corresponding to the time that particular spectral region remains in the coating, since the interference effects of the coating may occur at different depths in the multilayer for

different wavelengths. In the case of a 15-fs pulse, differences in the delay will lead to a temporal broadening of the pulse since some wavelengths will be reflected from the outer layers of the coating while others will be reflected from farther within the mirror. Through proper design of the coating, adjustments to the delay for different wavelengths may be made, for example, by the use of Gires–Tournois interferometer structure(s), resulting in coatings with positive, negative, or neutral dispersion.<sup>14</sup> Any significant delays incorporated in the optical coating, however, are typically the result of resonant cavities, leading to the amplification of the electric field intensity and likely resulting in a significant reduction in the laser-damage threshold of the coating.<sup>15–18</sup> By properly selecting the coating materials and minimizing the electric-field intensity in the lower-bandgap layers, one can achieve significant improvements in the laser-damage threshold of the coating.<sup>15–20</sup>

The shape of the wavelength-dependent GDD is also an important consideration for pulse compression since low-order phase profiles may be able to be compensated by tuning the combination of the stretcher and compressor in an OPCPA system.<sup>21</sup> Furthermore, GDD ripple of one mirror may be reduced by using another compensating mirror with the inverse ripple in the GDD.<sup>22–24</sup> This requires a systems-level approach for optical coating design since a given GDD magnitude or profile may or may not be acceptable, depending on the other components in the system, and whether the dispersion is purely additive or if there are coatings that cancel accumulated dispersion. Such components, if they contain higher electric-field intensities as a result of resonant cavities, may be placed in positions of low electric-field intensity prior to pulse amplification to offset the dispersive properties of coatings in high-fluence regions of the system.

A primary challenge for the production of coatings for femtosecond applications remains the deposition of such coatings for large-aperture applications, given that most femtosecond coatings are produced by ion-beam or magnetron sputtering.<sup>16,25–27</sup> Precision deposition for large-area coatings is generally performed by electron-beam evaporation as a result of the relative ease of scaling the coating process; while some femtosecond coatings have been demonstrated using evaporation processes, low-dispersion, high-damage-threshold coatings suitable for use in a meter-class laser system have not been thoroughly investigated.<sup>28,29</sup> To maintain acceptable wavefront performance and dispersion characteristics of the coatings, thickness uniformity and thin-film stress must be controlled over the aperture of interest while limiting film defects that may lead to reduced laser-damage thresholds.<sup>13,30–32</sup>

To meet the spectral bandwidth of a coating, a quarter-wave reflector is typically constructed of alternating high- and low-index materials; the width of the reflector at normal incidence is given by

$$\Delta g = \frac{2}{\pi} \sin^{-1} \left( \frac{n_H - n_L}{n_H + n_L} \right), \quad (1)$$

where  $\Delta g$  is the half-width of the reflector in normalized frequency,  $n_H$  is the refractive index of the high-index material, and  $n_L$  is the refractive index of the low-index material.<sup>33</sup> The upper and lower normalized frequency bounds of the reflector are then given by

$$g_{\text{edge}} = 1 \pm \Delta g \quad (2)$$

with the corresponding wavelengths of the reflector edges given by

$$\lambda_{\text{edge}} = \lambda_0 / g_{\text{edge}}. \quad (3)$$

Using coating materials suitable for the visible spectrum and a center wavelength of 910 nm, the width of a reflector using  $n_H = 2.2$  and  $n_L = 1.45$  is insufficient to maintain high reflectance and low GDD for the spectral extent of a 15-fs pulse. At near-normal incidence, the design complexity must become much greater by using multiple reflectors or a geometric stack in order to achieve the desired bandwidth, leading to greater difficulties in obtaining the desired group delay for one spectral region relative to another. To achieve the desired bandwidth, a larger difference in refractive index (which is not available) must be used or the coating must be used in *s*-polarization at oblique incidence since the width of the reflector increases as the incidence angle increases. The use of a greater  $\Delta n$  for the layers of the reflector coating, where  $\Delta n$  is defined as  $n_H - n_L$ , leads to a broader reflectance band for a quarter-wave reflector as does the use of *s*-polarization at higher angles of incidence. As shown in Fig. 136.10, the use of a niobia ( $n_H = 2.20$ )/silica ( $n_L = 1.45$ ) reflector provides a significantly broader reflectance band than if hafnia ( $n = 2.05$ ) is used as the high-index material, although based on the work of Mangote *et al.*, the expected laser-damage resistance is less than half that of hafnia.<sup>20,33</sup>

### Experiment

An initial series of dielectric coatings were prepared in a cryo-pumped, 54-in. coating chamber equipped with quartz heater lamps, dual electron-beam guns, multipoint quartz crystal monitoring, and planetary substrate rotation. Granular

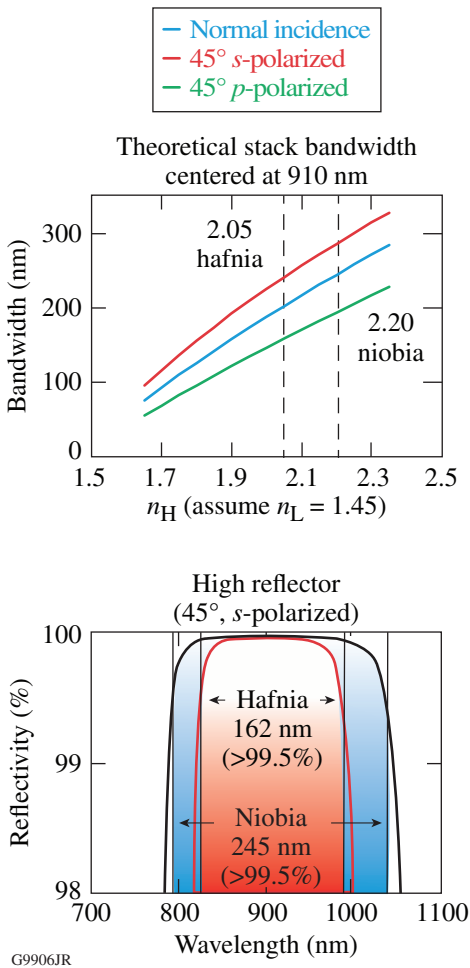


Figure 136.10

(a) Dependence of a high-reflector stack width on  $n_H$ , assuming  $n_L = 1.45$ , for normal and 45°-incidence use. (b) Theoretical width of an *s*-polarized reflector at 45° incidence is significantly broader for a niobia/silica coating than for a hafnia/silica coating. Using the reflector in *s*-polarization at high incidence angles broadens the reflectance band, while using *p*-polarization narrows the usable spectral bandwidth.

silicon dioxide was evaporated from a continuously rotating pan, while niobium, hafnium, silver, copper, and aluminum oxide were deposited from a six-pocket electron-beam gun. A Thin Film Solutions plasma source was installed in the chamber to provide densification and more-complete oxidation of the niobium and hafnium. The plasma source was operated with a beam voltage of 160 V with a 35-A discharge current for deposition of dielectric coatings with an oxygen flow of 55 sccm introduced through the process gas ring above the plasma source. The plasma source was reduced to a 5-A discharge current with no oxygen flow for deposition of metal layers as well as the first 15 nm of alumina deposited over the silver to minimize oxidation of the silver surface.

To meet the required spectral bandwidth using a traditional quarter-wave reflector, different material combinations, angles of incidence, and polarizations were evaluated. For an all-dielectric solution, it was determined that a 45°-incidence, *s*-polarized quarter-wave reflector fabricated with refractive indices of 2.20 ( $\text{Nb}_2\text{O}_5$ ) and 1.45 ( $\text{SiO}_2$ ) would be sufficient to meet the 810- to 1010-nm bandwidth with relatively low dispersion effects. Using a high-index material with a refractive index of less than 2.20 would require a greater angle of incidence with a corresponding larger substrate or a more-complex design to broaden the reflectivity while controlling the dispersion properties, typically resulting in higher electric-field intensities and an associated reduction in damage thresholds. To provide broader bandwidths, *p*-polarized reflectors, and lower-incidence angles, more-complex dielectric coatings with potentially higher GD, GDD, and electric-field intensity may be considered, or it will become necessary to use coatings based on a metal reflector.

Coating deposition for the all-dielectric coatings was performed at a substrate temperature of 120°C to stabilize the deposition temperature in the presence of heating from the electron-beam guns and plasma source. Niobia and hafnia were deposited at a deposition rate of 0.12 nm/s, silica at 0.4 nm/s, and alumina at 0.2 nm/s. Metal coatings were deposited at ambient temperature, with the only substrate heating resulting from the deposition and plasma sources. Copper was deposited at 1 nm/s, while silver was deposited as quickly as possible for maximum reflectance without ejection of defects from the source, which was determined to be  $\sim 1.8$  nm/s.

The positions of the electron-beam guns and planetary rotation geometry were configured for uniform deposition over the substrate aperture without the use of uniformity masks; the goal was to limit phase discontinuities in the coating resulting from disruptions in the vapor plume caused by uniformity masking.<sup>30,34</sup> A custom planetary rotation was designed and fabricated with three 13-in. planets alternating with three 4-in. planets designed for through-planet optical monitoring as shown in Fig. 136.11. All components were fabricated with precise manufacturing tolerances to ensure minimal thickness errors from differences in planet height or angular tilt with respect to the planet axis of rotation. The smaller-diameter rotation system makes higher revolution speeds possible, ensuring greater averaging of the deposition and a more-uniform coating. Comparable performance could also be achieved by reducing the deposition rate of the dielectric materials if it became necessary to coat larger substrates that could not practically be rotated at such high speeds.

Coating designs of alternating niobia and silica layers were selected to flatten GDD, minimize the standing-wave electric-field intensity, and achieve a compromise between the two goals. The influence of film nonuniformity was also evaluated by theoretically propagating a pulse through a system

containing 25 identical mirrors with 1% uniformity errors. The theoretical performance of the coating designs is shown in Figs. 136.12(a)–136.12(c). Adjustments to the stretcher/compressor angles and distances provide for up to third-order phase-error compensation; consequently, coating designs that

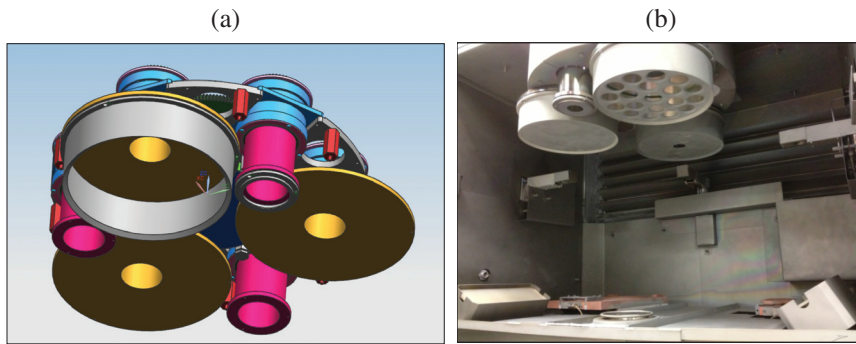
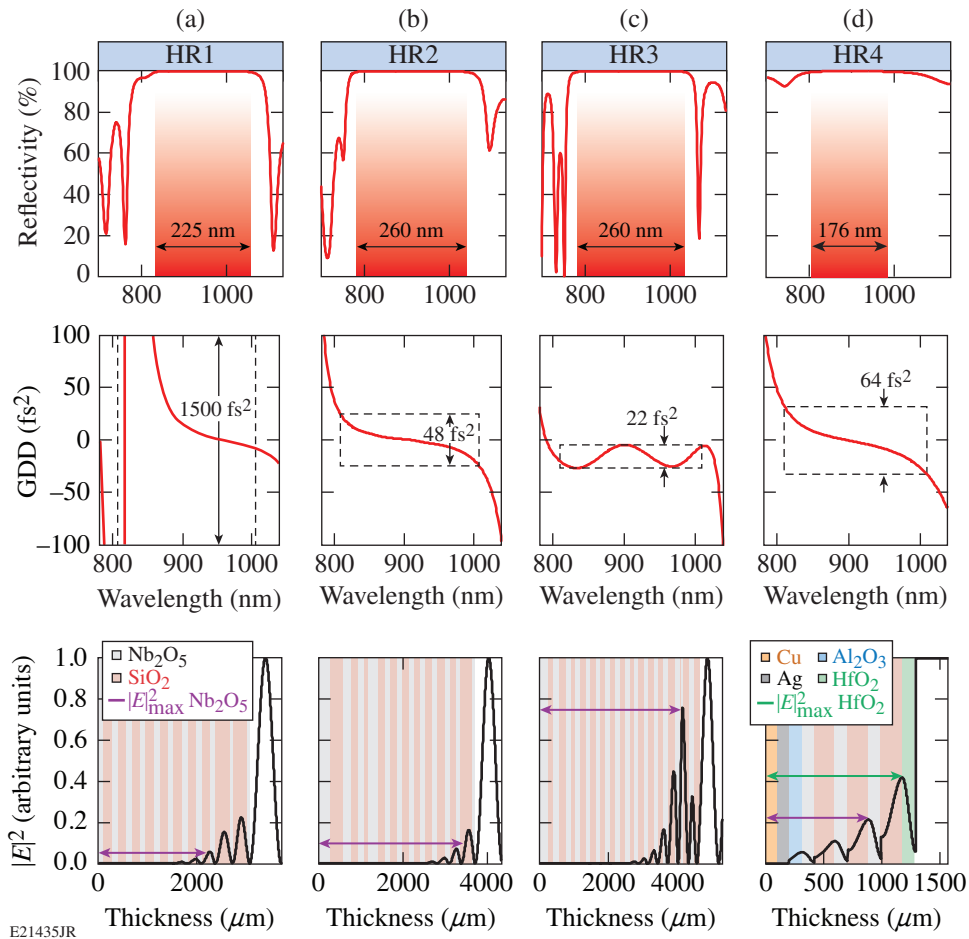


Figure 136.11

(a) Design of a precision planetary rotation system for high-speed rotation of substrates up to 310 mm in diameter, as well as the (b) fabricated rotation installed in a 54-in. coating diameter. Substrate planets alternate with 100-mm planets, making through-planet optical monitoring possible. System geometry is configured for uniform deposition over the substrate aperture without the use of shadow masks.

G9899JR



E21435JR

Figure 136.12

Theoretical reflectance, group-delay dispersion, and standing-wave electric-field intensity within the coating structure for HR1–HR4. Note that HR1–HR3 are for *s*-polarization, while HR4 is for *p*-polarized usage. Reflectance bandwidth is indicated for  $R > 99.5\%$ .

provide a phase-on reflection that closely fits a third-order polynomial are preferred to designs with less dispersion containing higher-order phase terms.<sup>21</sup>

While the all-dielectric design meets the specifications for an *s*-polarized reflector, a *p*-polarized reflector is also required. No low-GDD, all-dielectric design has been identified that is expected to maintain high laser-damage thresholds, owing to the enhanced electric-field intensities within the coating structure required for dispersion control. Instead, an enhanced silver coating was developed, as shown in Fig. 136.12(d). A copper underlayer was incorporated between the substrate and the silver layer to improve environmental durability; the dielectric enhancement layers consist of alumina (adhesion to the silver), niobia/silica (maximum  $\Delta n$  for reflectivity and spectral bandwidth), and hafnia (laser-damage resistance in the highest electric-field intensity).<sup>35</sup> The design for this coating can be expressed as

$$\text{substrate/Cu Ag A (NS)}^3\text{H/air}, \quad (4)$$

where A, N, S, and H represent nominally one quarter-wave optical thickness of alumina, niobia, silica, and hafnia, respectively, and the superscript “3” denotes a repetition of the included layers. The theoretical performance of such a coating meets reflectivity and dispersion requirements, with laser-damage thresholds remaining as the primary concern. For comparison, a protected silver mirror with a nominal half-wave optical thickness of alumina as well as an enhanced silver mirror with two hafnia/silica pairs of enhancement layers were also deposited.

These coatings are being developed for use with a 15-fs pulse having a spectral bandwidth of 810 to 1010 nm; however, a laser-damage test facility with this capability has not been identified. As a result, laser-damage thresholds have been evaluated with a number of different systems, with different center wavelengths, temporal pulse lengths, use environment, and evaluation criteria. The primary testing for femtosecond-coating performance was performed by Lidaris (formerly VULRC, Vilnius University) with an 800-nm laser and a 59-fs pulse. Damage testing was also performed at LLE by systems at 1053 nm with 1-ns, 10-ps, and 0.6-ps pulse durations, with testing at the nanosecond- and picosecond-pulse durations in accordance with the protocols described by Papernov and Howard, respectively.<sup>36,37</sup> In all cases, coating designs were adjusted from a nominal 910-nm center wavelength to center the coating performance at the wavelength being tested. All laser-damage thresholds are reported as the fluence of the inci-

dent beam; i.e., as the coating surface is adjusted to a greater angle of incidence relative to the incident laser, the beam fluence remains constant while the fluence on the surface is decreased by the cosine of the angle of incidence.

Accurate dispersion measurement was also not available at LLE. Sample coatings were evaluated with a beta version of a KMLabs *Chromatis* white-light interferometer for characterizing GDD. Measurements were compared to expected theoretical performance using this system, and further characterization will be pursued as possible. Initial results showed that HR2 and HR3 performed consistent with the theoretical GDD shown in Fig. 136.12, with an estimated measurement accuracy of  $\pm 10 \text{ fs}^2$ .

## Results

Source positions for niobium and silicon dioxide were optimized individually to provide uniform deposition over the substrate aperture by adjusting the radial distance from the chamber center and the source height, with multilayer uniformity evaluated based on the performance of a modified Grezes–Besset stack as described by Baumeister.<sup>38</sup> Optimal source positions were found to be 520 mm from center for niobium with a source-to-substrate distance of 606 mm, while the silica source was located 509 mm from chamber center with a source-to-substrate distance of 584 mm. The slight difference in optimal source position can be attributed to differences in the vapor plume shape of the two materials, as well as the extended size of the silica source relative to the small spot evaporation of the niobium. The multilayer thickness uniformity based on measurements of five samples distributed over a 254-mm aperture was determined to be  $\pm 0.04\%$  by characterizing a best fit of the spectral data in OptiRE shown in Fig. 136.13 (Ref. 39). The uniformity was found to be sensitive to changes in source height of the order of 1 to 2 mm, requiring significant care in the loading of sources particularly for silicon dioxide granules, which were  $\sim 3$  mm in size.

Samples of HR1–HR4 as described in Fig. 136.12 were deposited on 50.8-mm-diam fused-silica substrates. Analysis of the coating performance included simulations of the effects of the coating on a theoretical system containing 25 mirrors, assuming second- and third-order dispersion effects could be compensated by tuning the stretcher/compressor combination. Figure 136.14 shows the impact on the temporal pulse shape assuming a system of 25 identical mirrors for each of the coating designs. HR2 has a moderate amplitude with a low-order dispersion that can be compensated through stretcher/compressor adjustments.

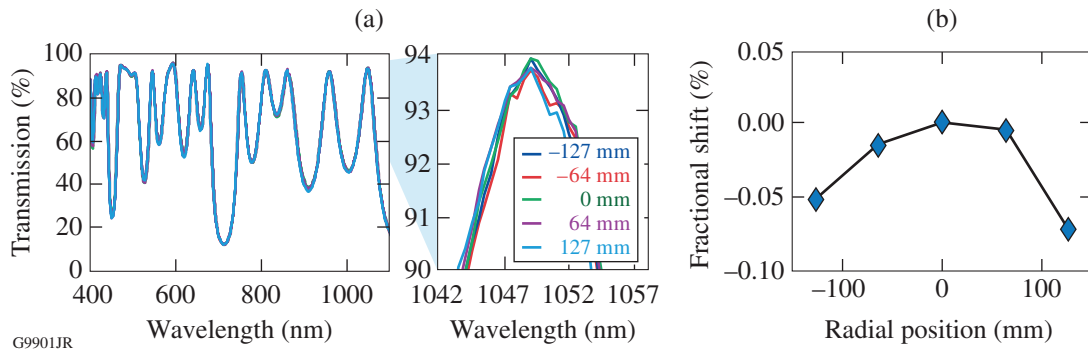


Figure 136.13 Measured thin-film uniformity over a 254-mm aperture based on system geometry. (a) Overlay of the spectral transmittance shows a negligible variation in coating performance among the samples. (b) Curve fitting and normalization of film thickness indicate film nonuniformity is of the order of  $\pm 0.04\%$ . Thickness variations are slowly varying, with minimal phase errors since the film deposition is continuous with no shadow masks between the source and substrate.

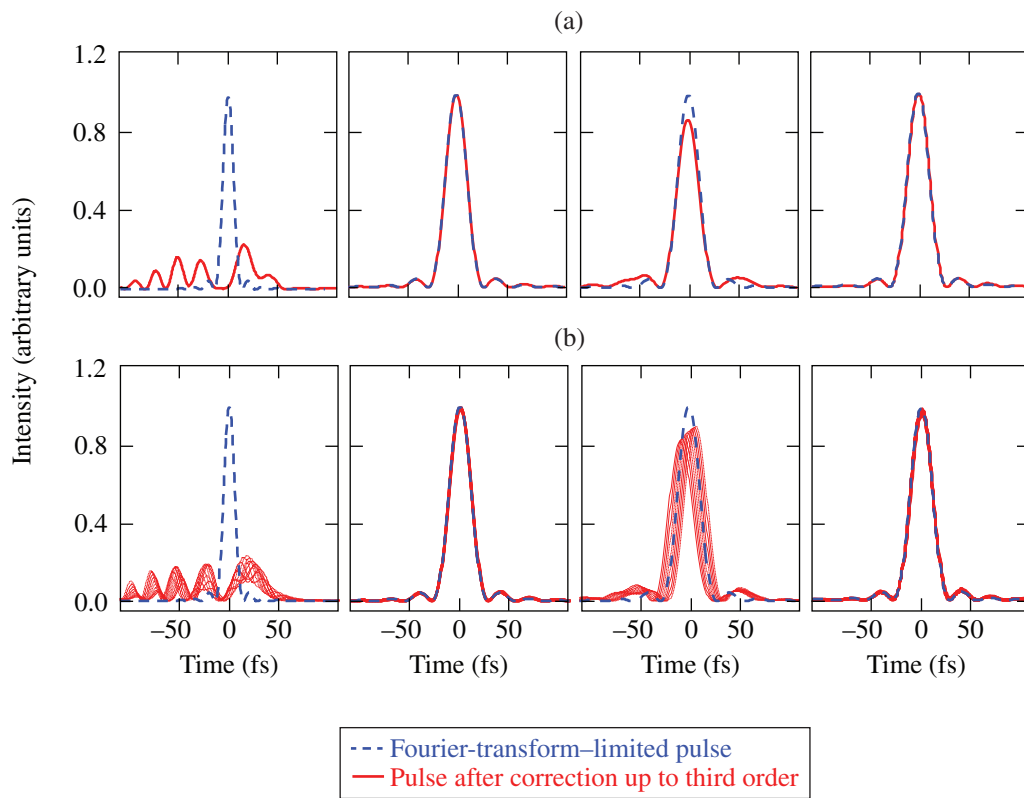


Figure 13.14 Impact on the temporal pulse shape for a theoretical system containing 25 mirrors of HR1, HR2, HR3, and HR4. The second- and third-order phase error resulting from dispersion is removed, based on the assumption that such error can be compensated by stretcher/compressor tuning. The performance in (a) is based strictly on the dispersion of the mirrors, while (b) assesses the impact of 1% film thickness nonuniformity over the mirror aperture.

Laser-damage testing by Lidaris at 59 fs required deposited coatings that were spectrally centered at an 800-nm wavelength to align with the test capability. The nominal  $S:1$  laser-damage thresholds (beam fluence) of HR1, HR2, and HR3 were measured to be  $1.64 \text{ J/cm}^2$ ,  $1.16 \text{ J/cm}^2$ , and  $0.12 \text{ J/cm}^2$ , respectively,

indicating a strong correlation with the maximum electric-field intensity in the niobia layers, as shown in Fig. 136.15. Based on the work of Mero *et al.*, it is expected that use with a 15-fs pulse will result in a reduction of the damage threshold of approximately  $1/3$ , using a  $\tau^{0.3}$  scaling law.<sup>40</sup>

The laser-damage threshold of the enhanced silver coating HR4 is also shown in Fig. 136.15, with its performance at  $0.69 \text{ J/cm}^2$  remaining consistent with that of HR1–HR3 based on the electric-field intensity in the outer high-index layers. Note that the damage threshold of HR4 is higher than expected [above the dashed line in Fig. 136.15(b)] based on the electric-field intensity in the outermost layer, which is hafnia, but this would correspond to the larger bandgap of hafnia relative to that of niobia in HR1–HR3, in agreement with the findings of Mangote *et al.*<sup>20</sup>

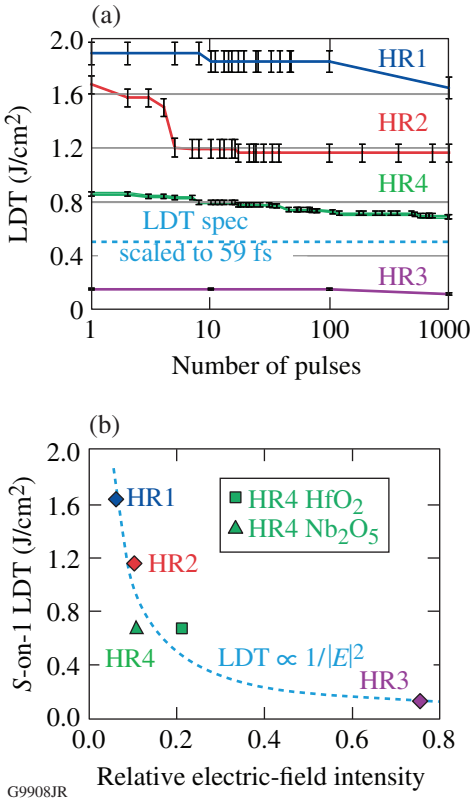


Figure 136.15 (a) Laser-damage thresholds (LDT's) of HR1–HR4 as tested by Lidaris using a 59-fs pulse with a center wavelength of 800 nm. (b) The performance of each coating is consistent with its relative electric-field intensity in the air-side high-index layer, indicating the damage is driven by the low electronic bandgap of the high-index material. Manipulation of the relative intensity of the electric field provides higher damage thresholds in HR1 and HR2.

Based on the performance of HR4 as a *p*-polarized reflector and the inherent broad reflectance and low GDD, two additional silver-based coatings were evaluated. Evaporated Cu/Ag metallic coatings were overcoated with a half-wave optical thickness of alumina (substrate/Cu Ag 2A/air) as well as enhanced with two dielectric pairs of layers (substrate/Cu Ag AHSH/air),

where A, H, and S are as defined previously. As the number of layer pairs in the dielectric overcoat is reduced, the reflectivity, in general, is decreased but the GDD is improved, approaching  $0 \text{ fs}^2$  for a layer of bare silver. As shown in Fig. 136.16, the laser-damage performance of the silver mirrors remains similar, with HR4 shown to have the lowest average damage threshold of the three mirror designs. As additional dielectric enhancement layers are added, the electric-field intensity at the silver layer is reduced, with an expected improvement in laser-damage threshold; since the hafnia-overcoated metal mirrors consistently have the highest laser-damage threshold, it appears the damage threshold remains a function of the bandgap of the high-index dielectric layer and not the metallic layers beneath.

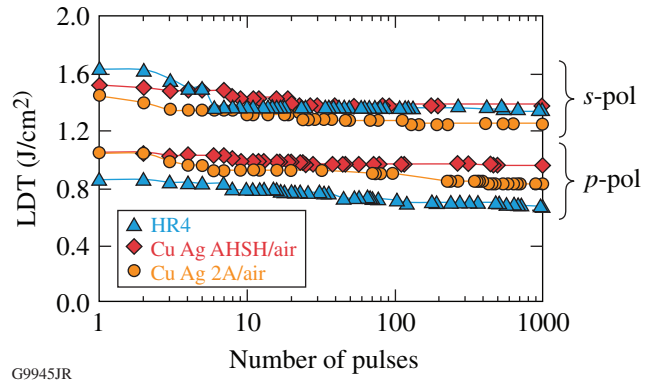


Figure 136.16 Laser-damage thresholds of silver-based mirrors as tested by Lidaris using a 59-fs pulse with a center wavelength of 800 nm. Damage thresholds for *s*-polarization remain consistently higher than those for *p*-polarization.

This work is intended for use over large apertures, with initial coating requirements for a 254-mm aperture, and ultimate potential needs of the order of a 1-m aperture. Based on the results above concerning temporal pulse shape and laser-damage threshold, HR2 was selected for demonstration on a larger-aperture substrate. The coating was deposited on a 310-mm-diam by 14-mm-thick fused-silica substrate, with a surface deviation of less than  $\lambda/10$  from flat. The primary concerns for scale-up include spatial irregularities in the reflected phase leading to variations in GDD and surface flatness, with minimal variation in reflectivity assured, given the measured film-thickness nonuniformity. The HR2 coating was deposited and the reflected wavefront performance was measured on an 18-in. phase-shifting Zygo interferometer operating at 1064 nm. The wavefront performance is shown in Fig. 136.17.

The optical power of 1.76 waves at 1064 nm, as measured in Fig. 136.17(b), corresponds to a thin-film stress of the order of 150 MPa based on Stoney's equation. A flatter coated surface

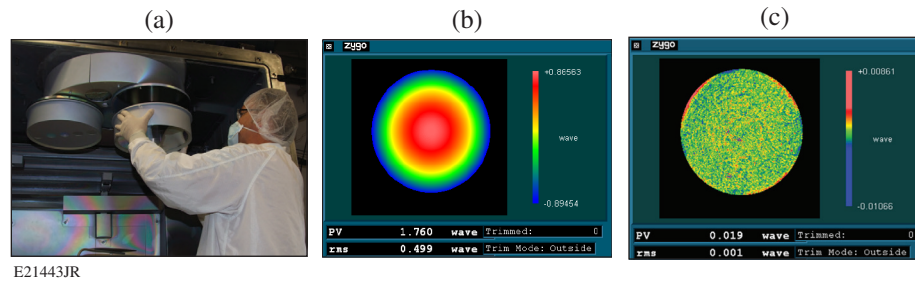


Figure 136.17

(a) The deposition process was demonstrated on a 310-mm-diam substrate, with (b) the flatness of the coated substrate in  $\sim 150$  MPa of thin-film stress. (c) Removal of the stress-induced surface deformation results in a remaining spatial phase error of a random speckle pattern below the resolution of the interferometer.

may be realized by increasing the substrate thickness or depositing a compensating coating on the rear surface of the optic. As shown in Fig. 136.17(c), removing the stress-induced power and astigmatism from the wavefront map leads to a wavefront error indistinguishable from the noise of the interferometer resolution, with no discernible pattern indicative of spatial phase error from the substrate rotation, shadows, or other irregularities in the coating process. This shows that the deposition process provides a smooth optical phase-on reflection suitable for use with femtosecond optical pulses.

**Future Work**

Development of improved high-reflector coating designs is continuing, based on minimizing the electric-field intensity in high-refractive-index layers, maximizing the electronic bandgap of all coating materials in regions of high electric-field intensity, and controlling GDD as possible with metallic layers. Magnetron sputtering of metallic coatings will be evaluated as a means of limiting film defects for silver and copper deposition.

Remaining optical-coating challenges to be demonstrated for construction of the MTW-OPAL laser include a beam combiner/separator for the pump and signal beams as they enter and exit the nonlinear crystals for amplification of the signal pulse. To minimize the impact on GDD, a configuration transmitting the signal and reflecting the 527-nm pump laser has been selected for this dichroic filter. Operating at Brewster’s angle for a  $p$ -polarized signal beam and an  $s$ -polarized pump beam eliminates the need for a second-surface antireflection coating. In addition, a filter is also required to reject the idler beam (1100 to 1505 nm) resulting from the parametric amplification process. Since the signal must again be propagated without negatively impacting the spectral phase, a transmissive coating design was selected for this application, with the idler being reflected at  $56^\circ$  incidence in  $s$ -polarization, in order to provide a sufficiently broad spectral width of the reflectance

band and to reject the full spectrum of the idler beam. Measured performance of current demonstrations of these coatings is shown in Fig. 136.18, with both coating designs having a

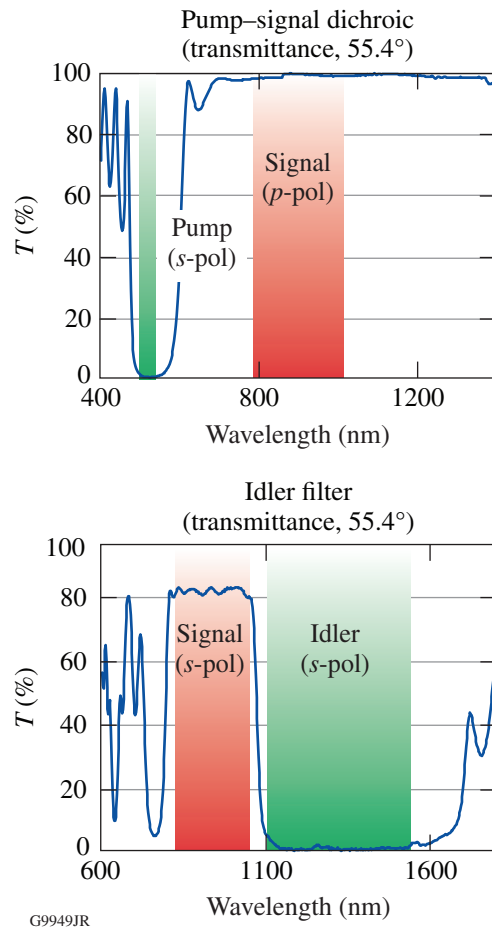


Figure 136.18

(a) Filters for the pump-signal combiner/seperator and (b) removal of the idler from the co-propagating signal beam. Performance of both filter types has been successfully demonstrated for small apertures.

negligible impact on the theoretical GDD of the signal beam in transmission.

A final challenge is the deposition of a reflective coating for the final focusing optic. As the pulse is focused onto target, the beam will be full fluence with a compressed, 15-fs pulse. Dispersion and nonlinear refractive index of optical glasses necessitates the use of a reflective focusing optic, although a radially dependent GD and GDD resulting from coating nonuniformity over the curved substrate surface may lead to broadening of the temporal pulse at the focus if a dielectric interference coating is used. Metallic coatings may not possess a sufficiently high laser-damage threshold for the highest-fluence region of the optical system. At this time, modifying the radial source position within the overall system geometry is being pursued to match the coating-thickness distribution over the curvature of the substrate surface. Current models indicate adjustments in source position relative to chamber center are sufficient to compensate expected film nonuniformity caused by substrate curvature. This will be pursued further once an optical system design has been completed for MTW-OPAL, specifying the dimensions and curvature of the final focusing optic.

### Conclusions

A process for producing plasma-assisted evaporated coatings with high reflectivity, high laser-damage thresholds, and controlled dispersion over large apertures has been developed. Demonstrated performance of an all-dielectric solution for a 45°-incidence, *s*-polarized reflector over a range of 810 to 1010 nm includes  $R > 99.5\%$ , a laser-damage threshold of  $>1.1 \text{ J/cm}^2$  (coating design shifted to be centered at 800 nm and tested with a 59-fs pulse), and a low-order (correctable) GDD  $< 50 \text{ fs}^2$ . It has been shown that laser-damage performance depends on the maximum electric-field intensity in the high-refractive-index layers, with improved performance for larger-bandgap high-index materials, such as hafnia. Film-thickness nonuniformity is less than 0.1% over a 254-mm aperture, with spatial phase errors remaining well controlled, successfully limiting the spatial-dependent mirror dispersion. Such a coating is suitable for the propagation of 15-fs pulses with negligible degradation of the transform-limited pulse shape, based on temporal modeling with stretcher/compressor compensation.

Near-normal incidence and 45°-incidence, *p*-polarized reflectors have been demonstrated using protected and enhanced silver coatings. The dispersion performance of an enhanced silver coating is much better than that of the all-dielectric solution, with comparable reflectivity; while *p*-polarized damage thresholds are lower, *s*-polarized performance of

the metallic coatings is comparable or better than that shown by the all-dielectric films. The performance achieved is readily scaled from the 254-mm aperture demonstrated to larger optics, using plasma-assisted evaporation coating systems.

### ACKNOWLEDGMENT

This material is based upon work supported by the Department of Energy National Nuclear Security Administration under Award Number DE-NA0001944, the University of Rochester, and the New York State Energy Research and Development Authority. The support of DOE does not constitute an endorsement by DOE of the views expressed in this article.

### REFERENCES

1. O. Chekhlov *et al.*, in *High Power Lasers for Fusion Research II*, edited by A. A. S. Awwal (SPIE, Bellingham, WA, 2007), Vol. 6735, Paper 67350J.
2. J. P. Chambaret *et al.*, in *Solid State Lasers and Amplifiers IV, and High-Power Lasers*, edited by T. Graf *et al.* (SPIE, Bellingham, WA, 2010), Vol. 7721, Paper 77211D.
3. G. Overton, *Laser Focus World* **48**, 15 (2012).
4. G. A. Mourou *et al.*, *Plasma Phys. Control. Fusion* **49**, B667 (2007).
5. J. Bromage, C. Dorrer, M. Millecchia, J. Bunkenburg, R. Jungquist, and J. D. Zuegel, in *Conference on Lasers and Electro-Optics 2012*, OSA Technical Digest (online) (Optical Society of America, 2012), Paper CTh1N.7.
6. J. H. Campbell *et al.*, in *Optical Engineering at the Lawrence Livermore National Laboratory II: The National Ignition Facility*, edited by M. A. Lane and C. R. Wuest (SPIE, Bellingham, WA, 2004), Vol. 5341, pp. 84–101.
7. J. B. Oliver, J. Howe, A. Rigatti, D. J. Smith, and C. Stolz, in *Optical Interference Coatings*, OSA Technical Digest Series (Optical Society of America, Washington, DC, 2001), Paper ThD2.
8. B. Pinot *et al.*, in *Laser-Induced Damage in Optical Materials 2001*, edited by G. J. Exarhos *et al.* (SPIE, Bellingham, WA, 2002), Vol. 4679, pp. 234–241.
9. E. Lavastre *et al.*, in *Optical Interference Coatings*, OSA Technical Digest Series (Optical Society of America, Washington, DC, 2004), Paper TuF3.
10. J. B. Oliver, T. J. Kessler, H. Huang, J. Keck, A. L. Rigatti, A. W. Schmid, A. Kozlov, and T. Z. Kosc, in *Laser-Induced Damage in Optical Materials: 2005*, edited by G. J. Exarhos *et al.* (SPIE, Bellingham, WA, 2005), Vol. 5991, Paper 59911A.
11. J. Bellum *et al.*, in *Laser-Induced Damage in Optical Materials: 2009*, edited by G. J. Exarhos *et al.* (SPIE, Bellingham, WA, 2009), Vol. 7504, Paper 75040C.
12. R. Thielsch *et al.*, *Thin Solid Films* **410**, 86 (2002).
13. J. B. Oliver, P. Kupinski, A. L. Rigatti, A. W. Schmid, J. C. Lambropoulos, S. Papernov, A. Kozlov, J. Spaulding, D. Sadowski,

- Z. R. Chrzan, R. D. Hand, D. R. Gibson, I. Brinkley, and F. Placido, *Appl. Opt.* **50**, C19 (2011).
14. R. Szipöcs *et al.*, *Opt. Lett.* **19**, 201 (1994).
15. C. K. Carniglia *et al.*, in *Laser Induced Damage in Optical Materials: 1983*, edited by H. E. Bennett *et al.*, Natl. Bur. Stand. (U.S.), Spec. Publ. 688 (U.S. Government Printing Office, Washington, DC, 1985), pp. 347–353.
16. K. Starke, T. Groß, and D. Ristau, in *Laser-Induced Damage in Optical Materials: 2000*, edited by G. J. Exarhos *et al.* (SPIE, Bellingham, WA, 2001), Vol. 4347, pp. 528–534.
17. S. Chen *et al.*, *Appl. Opt.* **51**, 6188 (2012).
18. J. H. Apfel, *Appl. Opt.* **16**, 1880 (1977).
19. J. B. Oliver, S. Papernov, A. W. Schmid, and J. C. Lambropoulos, in *Laser-Induced Damage in Optical Materials: 2008*, edited by G. J. Exarhos *et al.* (SPIE, Bellingham, WA, 2008), Vol. 7132, Paper 71320J.
20. B. Mangote *et al.*, *Rev. Sci. Instrum.* **83**, 013109 (2012).
21. S. Kane and J. Squier, *J. Opt. Soc. Am. B* **14**, 1237 (1997).
22. F. X. Kärtner *et al.*, *J. Opt. Soc. Am. B* **18**, 882 (2001).
23. F. X. Kärtner *et al.*, U.S. Patent No. US6,590,925 B1 (8 July 2003).
24. V. Pervak *et al.*, *Opt. Express* **17**, 7943 (2009).
25. F. X. Kärtner *et al.*, *Opt. Lett.* **22**, 831 (1997).
26. V. Pervak *et al.*, *Opt. Express* **16**, 10220 (2008).
27. V. Pervak *et al.*, in *Advances in Optical Thin Films II*, edited by C. Amra, N. Kaiser, and H. A. Macleod (SPIE, Bellingham, WA, 2005), Vol. 5963, Paper 59631P.
28. M. Bischoff *et al.*, in *Advances in Optical Thin Films II*, edited by C. Amra, N. Kaiser, and H. A. Macleod (SPIE, Bellingham, WA, 2005), Vol. 5963, Paper 59631N.
29. Z. Jinlong *et al.*, *Appl. Opt.* **50**, C388 (2011).
30. J. B. Oliver and D. Talbot, *Appl. Opt.* **45**, 3097 (2006).
31. C. J. Stolz *et al.*, in *27th Annual Boulder Damage Symposium: Laser-Induced Damage in Optical Materials: 1995*, edited by H. E. Bennett *et al.* (SPIE, Bellingham, WA, 1996), Vol. 2714, pp. 374–382.
32. C. J. Stolz, M. D. Feit, and T. V. Pistor, *Appl. Opt.* **45**, 1594 (2006).
33. H. A. Macleod, *Thin-Film Optical Filters*, 4th ed., Series in Optics and Optoelectronics, edited by E. R. Pike and R. G. W. Brown (CRC Press, Boca Raton, FL, 2010), pp. 222–223.
34. S. K. Yao, *J. Appl. Phys.* **50**, 3390 (1979).
35. D.-Y. Song *et al.*, *Appl. Opt.* **24**, 1164 (1985).
36. S. Papernov and A. W. Schmid, *J. Appl. Phys.* **82**, 5422 (1997).
37. H. P. Howard, A. F. Aiello, J. G. Dressler, N. R. Edwards, T. J. Kessler, A. A. Kozlov, I. R. T. Manwaring, K. L. Marshall, J. B. Oliver, S. Papernov, A. L. Rigatti, A. N. Roux, A. W. Schmid, N. P. Slaney, C. C. Smith, B. N. Taylor, and S. D. Jacobs, *Appl. Opt.* **52**, 1682 (2013).
38. P. Baumeister, *Optical Coating Technology* (SPIE Optical Engineering Press, Bellingham, WA, 2004), pp. 9-56–9-57.
39. A. V. Tikhonravov and M. K. Trubetskov, OptiLayer Thin Film Software, Optilayer Ltd., <http://www.optilayer.com> (9 June 2005).
40. M. Mero *et al.*, *Phys. Rev. B* **71**, 115109 (2005).